ACCSCIENCE PUBLISHING

Journal of Seismic Exploration

ARTICLE

Elastic modulus analysis of a 3D-printed permafrost simulation model with varying porosity in a seismic physical modeling

Daechul Kim[1], Yeonjin Choi[1], Wookeen Chung[2], and Sungryul Shin[2]*

[1]Division of Glacier and Earth Sciences, Korea Polar Research Institute, Incheon, Republic of Korea

[2]Department of Energy and Resources Engineering, College of Ocean Science and Engineering, National Korea Maritime and Ocean University, Busan, Republic of Korea

Abstract

Global warming is causing permafrost thawing, which can lead to permafrost collapse. Assessing the stability of permafrost against this collapse risk is essential. One effective approach to evaluating permafrost stability is to use the elastic modulus. Since the elastic modulus varies with the ice content in the pore spaces, analyzing its relationship with porosity is crucial for understanding permafrost stability. Previous studies have used rock cores to analyze the relationship between elastic modulus and porosity. However, the analysis of elastic modulus relative to various porosities in permafrost is limited. To overcome these limitations, porosity was controlled using 3D printing, and a permafrost analog model with seismic velocities and porosities similar to those of natural permafrost was fabricated and assumed as permafrost. To analyze elastic modulus as a function of porosity in permafrost, seismic velocities were measured through seismic physical modeling experiments, and the elastic modulus was estimated from the measured seismic velocities. Analysis of the relationship between elastic modulus and porosity revealed that the elastic modulus decreased after increasing to a specific porosity in the permafrost simulation model. These findings provide a quantitative basis for evaluating the stability of infrastructure on permafrost by demonstrating the significant effect of ice expansion on mechanical properties. Furthermore, this study validates the 3D printing approach as an effective tool to overcome the limitations of natural rock cores for systematic permafrost research.

Keywords: Seismic physical modeling; Permafrost; 3D printing; Porosity; Elastic modulus

***Corresponding author:**
Sungryul Shin
(srshin@kmou.ac.kr)

Citation: Kim D, Choi Y, Chung W, Shin S. Elastic modulus analysis of a 3D-printed permafrost simulation model with varying porosity in a seismic physical modeling. *J Seismic Explor*. doi: 10.36922/JSE025420091

Received: October 17, 2025

Revised: January 2, 2026

Accepted: January 16, 2026

Published online: March 6, 2026

1. Introduction

Permafrost is ground that remains below 0°C for at least 2 consecutive years, and covers about 15% of the Northern Hemisphere.[1,2] Permafrost stores a large amount of organic carbon, and its melting due to global warming can accelerate global warming by increasing emissions of greenhouse gases such as carbon dioxide and methane.[3,4] Specifically, the thawing of permafrost is causing ground collapse, damaging pipes, infrastructure, etc.[5] Therefore, permafrost analysis is necessary to predict and prepare for changes in permafrost caused by thawing to ensure stability. One method for analyzing permafrost stability is the elastic modulus.[6]

The permafrost pores are saturated with ice, leading to varying ice saturation relative to porosity. Because ice thawing within pores can cause ground collapse, analyzing the elastic modulus as a function of porosity is crucial for assessing and predicting the stability of permafrost under thawing. The elastic modulus of permafrost can be measured directly using destructive testing of core samples or indirectly using seismic velocity. To analyze seismic velocity relative to porosity in permafrost, core samples are measured in the laboratory, or well logging is performed. However, because permafrost varies regionally and is found in polar regions, obtaining samples with diverse porosities or conducting well logging is difficult. Therefore, prior research has used rock cores to simulate permafrost and analyze porosity and seismic velocity.[7-11] Recently, research has been conducted to fabricate frozen soil models using artificial porous sandstone samples and to estimate ice saturation.[12] Although rock core samples and artificial porous sandstone samples have the advantage of being media similar to the permafrost environment, there are limitations in controlling the pore size, structure, and porosity desired by researchers. In contrast, 3D printing enables the control of the porous model as desired by the researcher. If porosity can be controlled and its elastic modulus can be analyzed, this will help assess the stability of permafrost.

As a method to create 3D models by layering, 3D printing offers the advantage of producing porous models with complex structures. It can be classified into seven types based on the additive manufacturing method. These include material extrusion, vat photopolymerization, powder bed fusion, material jetting, binder jetting, direct energy deposition, and sheet lamination.[13] Studies have used 3D printing to create rock cores that simulate pores and analyzed their properties. Ishutov *et al.*[14] proposed a method for simulating the porosity of sandstone using 3D printing with material extrusion and vat photopolymerization. Meanwhile, Ibrahim *et al.*[15] compared and verified the porosity of 3D-printed rock cores with that of real rock cores using vat photopolymerization and material jetting.

Utilizing this 3D printing technique, porous models can be created by controlling porosity, and their properties can be analyzed based on that porosity. Seismic physical modeling is a method for measuring seismic velocity, a property of 3D-printed porous models. This technique utilizes actual propagating waves and elastic media. Although the ultrasonic frequency and model dimensions differ from those in field exploration, this method offers the advantage of analyzing wave propagation characteristics within a controlled laboratory environment. Recently, this method has been effectively applied to analyze the seismic response characteristics of P, shear-vertical (SV), and shear-horizontal (SH) waves to reservoir parameters and to study complex lithofacies and structures in shale oil reservoirs.[16,17]

Studies have utilized 3D printing to create porous models for seismic physical modeling, saturate the pores with fluid, and analyze the fluid. Huang *et al.*[18] and Huang *et al.*[19] analyzed seismic velocity by saturating water in a penny-shaped porous model made by 3D printing using the material extrusion method, while Dande *et al.*[20] analyzed seismic velocity and anisotropy as a function of fluid and viscosity in the same model. Dande *et al.*[21] and Wang *et al.*[22] fabricated porous models with fractures using 3D printing and analyzed the elastic wave characteristics of the fractures. Zerhouni *et al.*[23] and Kim *et al.*[24] used 3D printing to print porous models with varying pore sizes and analyzed the seismic properties with respect to porosity.

In seismic physical modeling, studies of porous models printed in 3D have primarily focused on saturating fluids and analyzing seismic velocities. The present study simulated permafrost by saturating the pores of 3D-printed porous models with varying porosities with ice. Seismic velocities were measured using the simulated permafrost models, and the corresponding elastic moduli were calculated to analyze how elastic modulus changes with porosity. The elastic modulus is one of the important physical properties in determining the stability of permafrost during thawing. The porosity of the permafrost simulation model was designed to fall within the permafrost porosity range, and the medium used was similar to the velocity of the strata that comprised the permafrost.

2. 3D-printed permafrost simulated model

2.1. Design and printing of a permafrost simulation model with similar porosity and P-wave velocity to permafrost

A permafrost simulation model was designed and 3D-printed. To ensure the model was similar to permafrost, the porosity and P-wave velocity were set to values similar to those reported in previous studies. Figure 1 summarizes previous studies on the porosity and P-wave velocity of permafrost. The porosity ranges from 10% to 60%, and the P-wave velocity was 2,000–6,000 m/s.[7-11] In the present study, permafrost simulation models were designed with porosities of 23.2%, 30.0%, 38.0%, and 42.7% to span the permafrost porosity range. The porosity was calculated as the ratio of the total volume to the volume of pores in the design. The porosity was controlled by varying the number of pores, and the pore size was kept constant at 2 mm. In addition, to facilitate water injection and ensure complete ice saturation within the pores, 0.5 mm

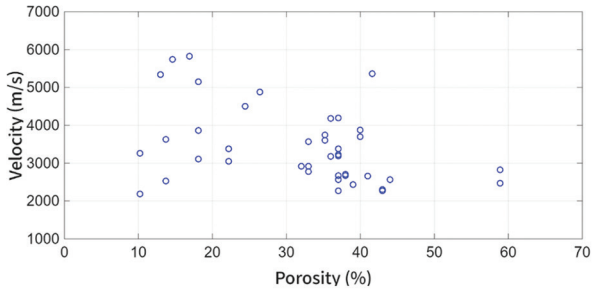

Figure 1. Permafrost porosity and P-wave velocity. Blue markers represent the P-wave velocity of permafrost as a function of porosity, as reported in prior research.[7-11]

channels were added to the X and Y faces, each connecting to every pore. Figure 2 presents the schematic design of the permafrost simulation models, detailing the internal structure, which features 2 mm pores and a network of 0.5 mm interconnecting channels on the X and Y faces to ensure effective fluid flow and complete saturation. Figure 2A represents Model 1, designed with a porosity of 23.2%, Figure 2B shows Model 2 with 30.0%, Figure 2C corresponds to Model 3 with 38.0%, and Figure 2D depicts Model 4 with 42.7%.

The designed permafrost simulation models were intended to be printed on a medium with a P-wave velocity similar to that of the permafrost. To measure the P-wave velocity of the polylactic acid (PLA) filament, a PLA solid model with each axis of 25 mm and a porosity of 0% was printed. Its P-wave velocity was measured using seismic physical modeling and was approximately 2,150 m/s.[25] Meanwhile, the velocity of ice-free sedimentary layers in permafrost areas was <2,500 m/s. As the P-wave velocity of the PLA filament was similar to that of the permafrost, the permafrost simulation models were 3D-printed with the PLA filament using fused deposition modeling (FDM) (Figure 3).[26] FDM is a representative additive manufacturing technology based on material extrusion, wherein a thermoplastic filament is heated to its melting point, extruded through a nozzle, and solidified on cooling to form successive layers.

2.2. Verification of the quality of the permafrost simulation model using porosity measurements

To verify the quality of the 3D-printed permafrost simulation models, porosities were measured. If it were measured similarly to the design model, it was thought that the porosity calculated in the design drawing and the porosity of the 3D-printed model would be similar. To measure the porosity of the permafrost simulation model, **Equation 1** was used:

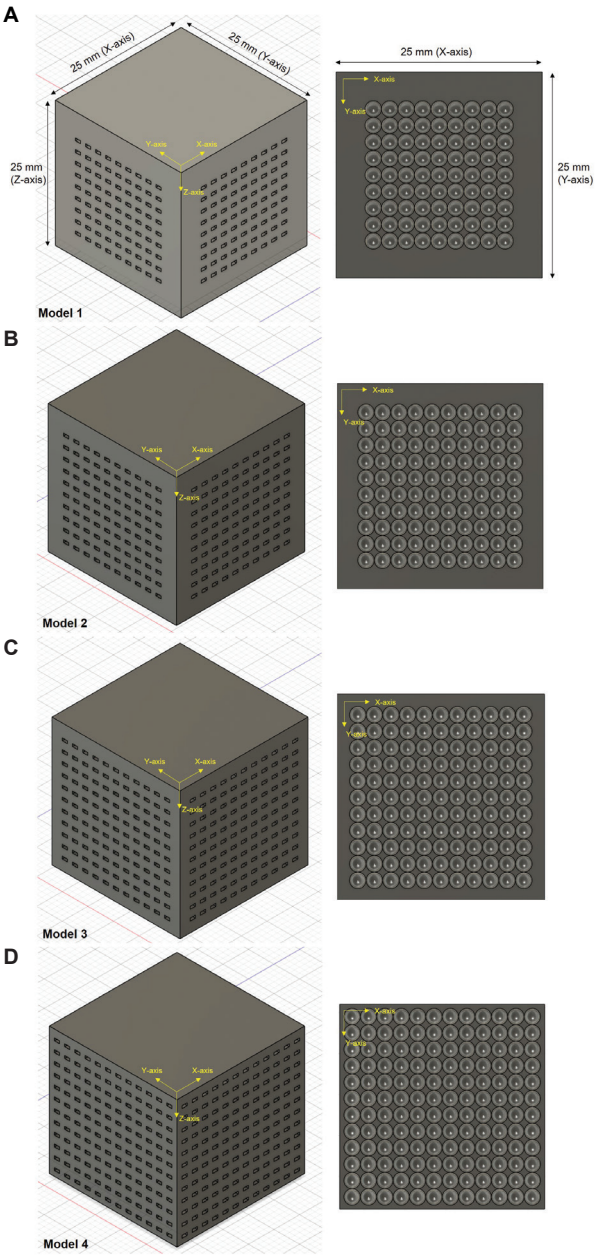

Figure 2. Permafrost simulation models designed with various porosities. (A) Model 1. (B) Model 2. (C) Model 3. (D) Model 4.

$$\varnothing = \frac{V_v}{V} \times 100\ (\%) \tag{1}$$

where $\varnothing$ is the porosity, V is the total volume of the model, and V_v is the void volume. V_v was calculated using **Equation 2**, and each parameter is listed in Table 1:

$$V_v = \frac{M - M_M}{\rho} \tag{2}$$

Table 1. Porosities of the permafrost simulation models and the parameters used for porosity calculation

Model	Measured porosity (Ø, %)	Mass without pores (M, g)	Mass with pores (M_M, g)	Total volume (V, cm³)	Void volume (V_v, cm³)	Density (ρ, g/cm³)
1	23.4	19.3	14.7	15.8	3.7	1.2
2	30.2	19.3	13.4	15.7	4.7	1.2
3	38.3	19.3	11.8	15.7	6.0	1.2
4	47.6	19.3	10.0	15.7	7.5	1.2

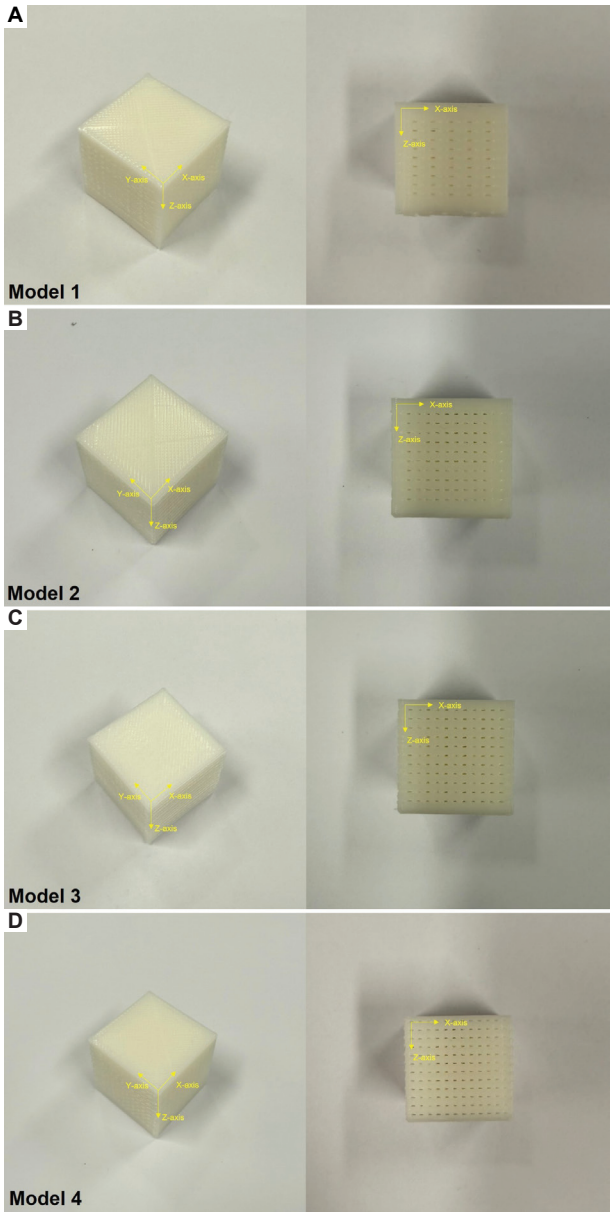

Figure 3. 3D-printed permafrost simulation models. (A) Model 1. (B) Model 2. (C) Model 3. (D) Model 4.

where M is the mass of the model without pores, M_M is the mass of the permafrost simulation model with pores, and ρ is the density of the model. The porosity measurements were 23.4%, 30.2%, 38.3%, and 47.6% for Models 1, 2, 3, and 4, respectively. These porosities were comparable to the corresponding calculated porosities, indicating the quality of the permafrost simulation models (Figure 4).

2.3. Permafrost simulation

To simulate the characteristics of permafrost within a 3D-printed model, a controlled water saturation process was implemented using a vacuum chamber and a vacuum pump. The purpose of this procedure was to ensure full saturation of the internal pore structures of the 3D-printed sample with water. As shown in Figure 5, the model was first immersed in water within the vacuum chamber. Subsequently, a vacuum pump was used to reduce the ambient pressure, thereby facilitating the infiltration of water into the internal pores by displacing entrapped air.

In this study, it is essential to ensure that the pore space within the permafrost simulation model is fully saturated with ice after freezing. To achieve this condition, the pores must first be completely saturated with water before the freezing process. Therefore, to verify the degree of saturation, porosity measurements were conducted at different time intervals during the saturation process. As illustrated in Figure 6, the measured porosity remained constant regardless of the saturation duration, and the values closely matched the initial porosity obtained through the method described in Section 2.2. This consistency indicates that the internal pores had been effectively and fully saturated with water. Hence, it was concluded that the sample reached full saturation, making it suitable for subsequent freezing and seismic physical modeling.

To simulate the formation of permafrost, the water-saturated porous model was subjected to a controlled freezing process by maintaining it at a temperature of −25°C for a duration of 24 h. During freezing, water within the pore spaces expands on phase transition to ice, which can exert internal stresses and potentially lead to structural deformation or cracking of the 3D-printed model. Therefore, a deformation control strategy was

implemented to prevent structural distortion of the model during the freezing process.

As illustrated in Figure 7, the model was mechanically constrained along the Z-axis using a vice to prevent vertical expansion. This fixation effectively minimized deformation in the vertical direction, where stress accumulation is most likely to occur due to gravity-assisted water distribution. In addition, the model was designed and positioned such that excess water, subjected to volume expansion on freezing, could be expelled laterally along the X- and Y-axes. By allowing this lateral release of pressure, the risk of internal damage and structural distortion within the model was significantly reduced. This approach ensured that the model retained its original shape and dimensions after freezing, thereby maintaining the reliability of the permafrost simulation and subsequent experimental analyses.

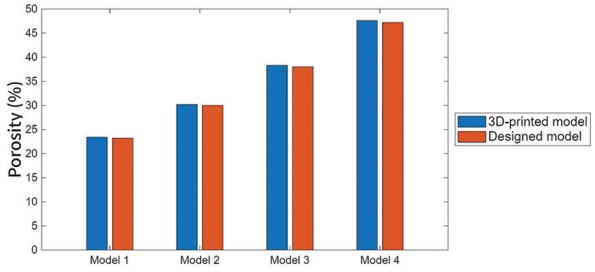

Figure 4. Comparison of measured and calculated porosities across permafrost simulation models

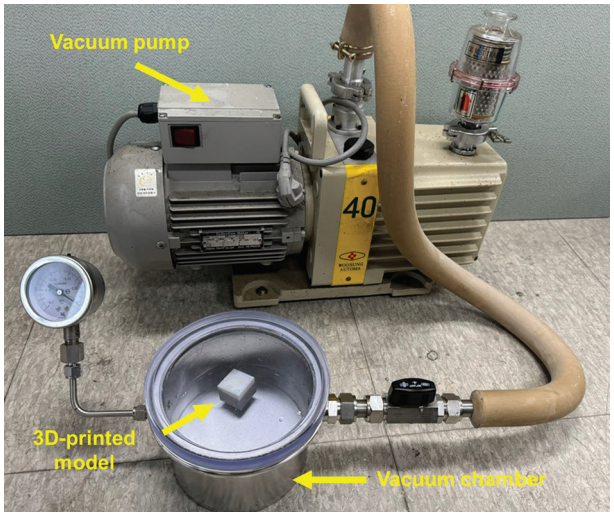

Figure 5. A system for saturating the pores of the 3D-printed models

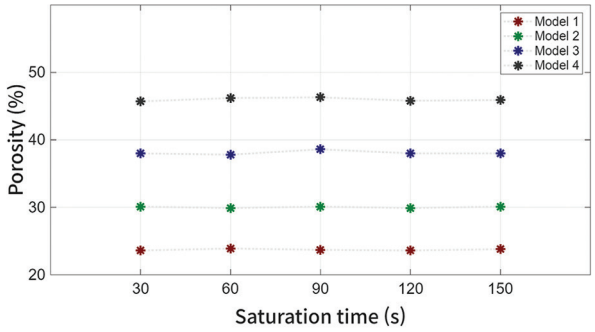

Figure 6. Porosity of 3D-printed models over saturation time

To verify that the pores within the 3D-printed permafrost model were fully saturated with ice after freezing, the porosity of the frozen model was measured. The measurement was conducted using the same method described in Section 2.2, and the results confirmed that the porosity was similar to the initial porosity before saturation (Table 2). Therefore, it was determined that the pores within the model were fully saturated with ice. The slight discrepancy in porosity measurements before and after freezing is an inevitable consequence of the freezing expansion of water. Although deformation was mechanically constrained along the Z-axis, the internal expansion pressure of the ice may have induced minor deformations in the PLA skeleton. However, these results confirm that the models were successfully saturated with ice without experiencing significant structural failure. Accordingly, the porosity measured after freezing was used for the research analysis. Further analysis linking these expansion-induced stresses to the observed elastic modulus behavior is provided in the discussion section.

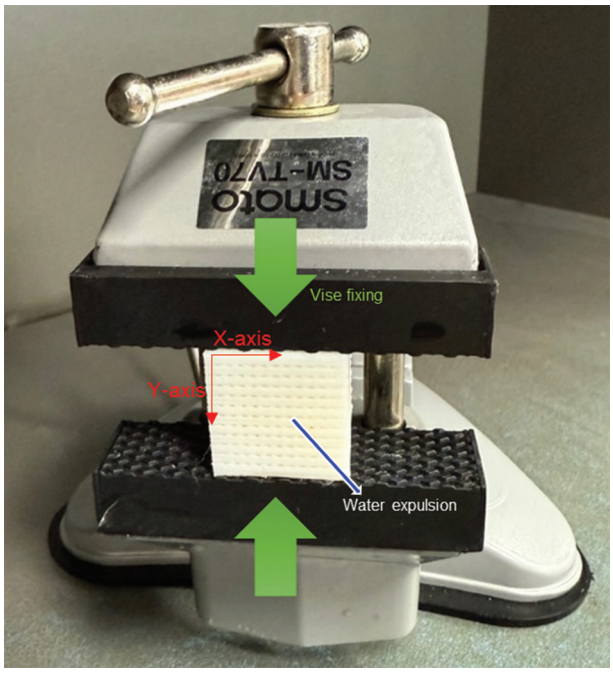

Figure 7. Preventing deformation of permafrost simulation models due to volume expansion

3. Seismic physical modeling

In this study, seismic physical modeling was conducted to estimate the elastic modulus of permafrost by measuring seismic velocities. This method enables the measurement of P-wave and S-wave velocities within a permafrost simulation model designed to replicate the porosity and seismic velocities of permafrost. A pulser/receiver system (5055PR, Panametrics, USA) was employed to generate and control the source signals, while a digital oscilloscope (MSOX2012A, Keysight, USA) was utilized for data acquisition, enabling precise recording of waveforms transmitted through the model. The overall experimental setup is illustrated schematically in Figure 8.

For wave generation and detection, 1 MHz P-wave and S-wave piezoelectric transducers (V103 and V153, for P-wave and S-wave, respectively, Olympus, USA) were used as the source and receiver. These transducers were carefully aligned along their respective propagation axes and firmly fixed in place to ensure consistent and repeatable signal transmission and reception. S-wave data were obtained by measuring both SH and SV wave components.

The SH-waves were acquired by positioning the S-wave transducer such that the vibration direction was perpendicular to the direction of wave propagation and parallel to the horizontal plane. To acquire SV-waves, the same S-wave transducer was rotated by 90° from the SH-wave orientation, thereby aligning its vibration direction vertically relative to the horizontal propagation path. This configuration allowed the separate characterization of different shear wave modes, which is essential for accurately estimating shear-related elastic moduli within the simulated permafrost model. Furthermore, measurements for each waveform were repeated five times to ensure reproducibility.

Figure 9 shows the P, SH, and SV wave waveforms obtained from the seismic physical modeling, and only the waveforms along the X-axis of Model 1 are shown as representative examples. The noise caused by the trigger at 0 μs was removed by muting.

Table 2. Comparison of measured porosity before and after freezing to verify ice saturation

Model	Measured porosity before freezing (%)	Measured porosity after freezing (%)
1	23.4	23.6
2	30.2	30.0
3	38.3	37.8
4	47.6	45.9

4. Elastic modulus analysis for porosity in permafrost simulation models

One method for analyzing the stability and condition of permafrost is to use the elastic modulus.[27,28] Therefore, to determine the stability of permafrost with respect to porosity, the elastic modulus was analyzed with respect to porosity. To analyze the elastic modulus for porosity in a permafrost simulation model, seismic velocities were calculated. The seismic velocities were derived from waveforms acquired, and the travel time from 0 μs to the signal and the model length were calculated. Table 3 shows the average P-wave and S-wave velocities, derived from five repeated measurements. The margin of error for these measurements ranged from 0.1% to 0.5%. The presence of elastic anisotropy within the permafrost simulation models can be confirmed from these velocity measurements. In general, the P-wave velocities showed distinct directional dependence, with horizontal velocities (X- and Y-axes) consistently exceeding the vertical velocity

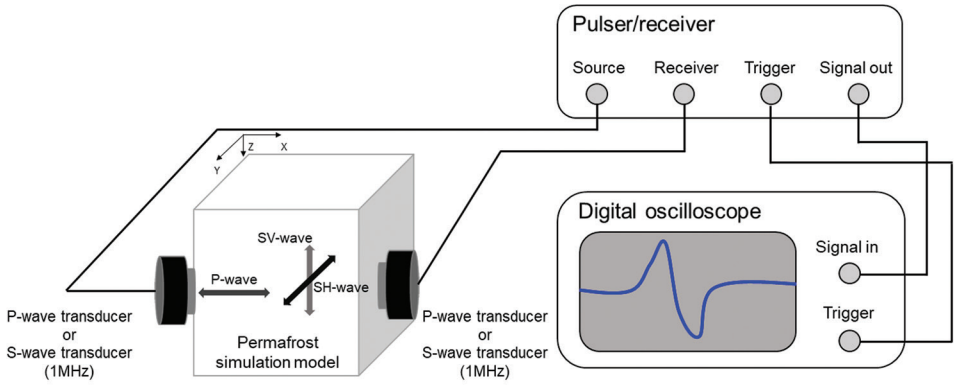

Figure 8. The schematic diagram of seismic physical modeling in the permafrost simulation model
Abbreviations: SH: Shear-horizontal; SV: Shear-vertical.

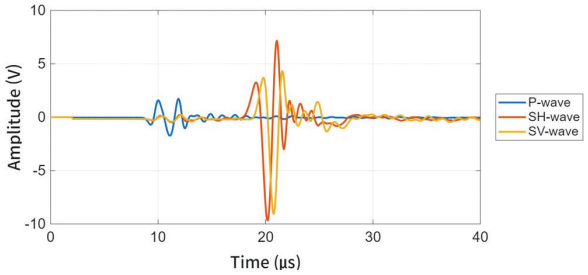

Figure 9. Waveforms of P, shear-horizontal (SH), and shear-vertical (SV) waves along the X-axis of Model 1

(Z-axis). Furthermore, significant shear wave splitting was observed, where SH-wave velocities were generally higher than SV-wave velocities. This anisotropy is attributed to the layer-by-layer manufacturing process of 3D printing, and it has been reported in previous studies using 3D-printed models.[19]

To verify the seismic physical modeling results, permafrost P-wave velocity and the Wylie equation for various porosities were compared (Figure 10). The Wyllie equation, a porous rock model for estimating porosity from seismic velocity, was used in this study to verify the velocity measurements with respect to porosity. This is because the measured seismic velocities must be accurate to be used in elastic modulus analysis. The Wyllie equation is shown in **Equation 3**[29]:

$$\frac{1}{V_p} = \frac{\varnothing}{V_f} + \frac{1-\varnothing}{V_m}.V_m \quad (3)$$

Where V_p is the P-wave velocity, $\varnothing$ is the porosity, V_f is the saturated fluid velocity, and V_m is the medium velocity.

To calculate the Wyllie equation, we acquired data from a 25 mm cube PLA solid model, identical to the permafrost simulation model, and seismic physical modeling data for ice (Figure 11). The cube PLA solid model has a 0% porosity and was measured after 24 h of freezing at −25°C, the same conditions as the permafrost simulation model. The velocities were 2,590.8 m/s, 2,578.0 m/s, and 2,552.3 m/s along the X-, Y-, and Z-axes, respectively. The average velocity of the three axes, 2,573.7 m/s, was used as V_m in the Wyllie equation. The ice velocity, 4,090.3 m/s, was measured under the same experimental conditions and was used as V_f. The verification results showed that the experimental results are within the velocity range of the permafrost in the seismic physical modeling and are consistent with the calculated results using the Wyllie equation.

The elastic moduli were calculated using the seismic velocities, which were the averages of five repeated

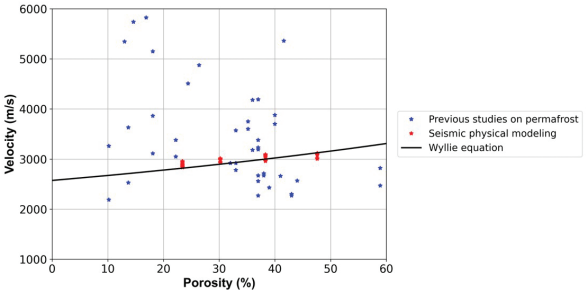

Figure 10. Graph demonstrating P-wave velocity against porosity. The permafrost velocities for various porosities shown in blue are referenced from Timur *et al.*,[7] Zimmerman and King,[8] Dou *et al.*,[9] Li and Matsushima,[10] and Kurfurst.[11] The red markers represent the P-wave velocities relative to porosity obtained from seismic physical modeling, while the black line indicates the theoretical results calculated using the Wyllie equation.

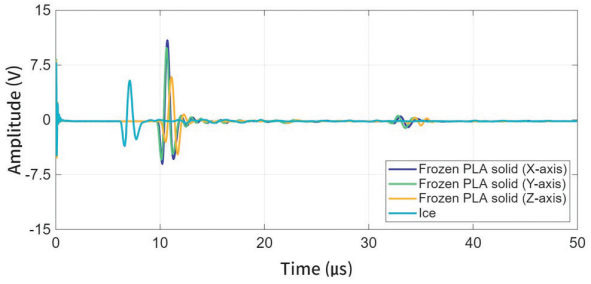

Figure 11. Reference P-wave waveform for calculating the Wyllie equation
Abbreviation: PLA: Polyactic acid.

Table 3. Seismic velocity for elastic modulus analysis in permafrost simulation models

Model	Axis	Porosity (%)	P-wave velocity (m/s)	SH-wave velocity (m/s)	SV-wave velocity (m/s)
1	X	23.6	2,942.1	1,410.1	1,342.2
	Y		2,883.9	1,399.9	1,328.2
	Z		2,842.9	1,343.0	1,330.3
2	X	30.0	3,001.7	1,431.0	1,370.1
	Y		2,990.8	1,428.0	1,356.3
	Z		2,928.0	1,375.2	1,376.2
3	X	37.8	3,085.7	1,472.3	1,414.0
	Y		3,043.0	1,463.6	1,423.3
	Z		2,967.2	1,409.8	1,410.3
4	X	45.9	3,110.2	1,484.6	1,444.7
	Y		3,087.7	1,481.9	1,428.4
	Z		3,010.3	1,439.6	1,428.7

measurements. Young's modulus (E), shear modulus (G), and bulk modulus (K) were calculated using **Equations 4-6**.[30]

$$E = V_p^2 \times \rho \quad (4)$$

$$G = V_s^2 \times \rho \quad (5)$$

$$K = \rho(V_p^2 - \frac{4}{3}V_s^2) \quad (6)$$

Where V_p is the P-wave velocity, ρ is the density, and V_s is the S-wave velocity. The resulting error ranges were 0.4–1.0% for Young's modulus, 0.2–0.7% for the shear modulus, and 0.4–1.4% for the bulk modulus.

Figure 12 shows Young's modulus as a function of porosity in a permafrost simulation model. The R^2 values displayed alongside the equations represent the coefficient of determination, indicating the goodness of fit for the regression models. As porosity increased, Young's modulus also increased, but then decreased at a porosity of approximately 38%. Figure 13 illustrates the shear modulus as a function of porosity, calculated using SH- (Figure 13A) and SV-wave (Figure 13B) velocity and density data obtained from seismic physical modeling. Shear modulus also increased with increasing porosity, then decreased at approximately 38%.

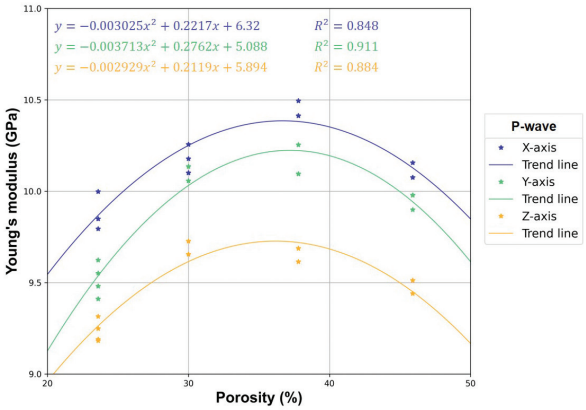

Figure 12. Young's modulus versus porosity in the permafrost simulation model. The trend lines were generated using a second-order polynomial. Blue, green, and yellow markers represent the Young's modulus measured along the X-, Y-, and Z-axes, respectively.

Bulk modulus was calculated using P-wave, S-wave, and density. The S-wave was calculated by distinguishing between the SH-wave and the SV-wave. Figure 14 presents the relationship between porosity and bulk modulus, where Figure 14A represents the results derived from SH-waves and Figure 14B represents those from SV-waves. As porosity increased, bulk modulus also increased and then gradually decreased.

In permafrost, the elastic modulus is affected by a combination of factors, including pore size, porosity, temperature, and the degree of ice saturation within the pore space. Among these, porosity and ice content play particularly important roles in determining the mechanical behavior of frozen ground. Previous studies have generally shown that when pores are fully saturated with ice, the elastic modulus tends to increase with increasing porosity, primarily due to the stiffening effect of ice within the pore network.[31,32]

However, in this study, non-linear trends were observed in the relationship between elastic modulus and porosity. Specifically, the elastic modulus increased with increasing porosity up to a certain threshold, beyond which it began to decrease. To understand this behavior, the analysis focused on how seismic velocity and density vary with porosity, along with the effects of freezing on these properties. This is because the elastic modulus was calculated using **Equations 4-6**, which are functions of both seismic wave velocity and material density.

Figure 15 presents the variation of both parameters as porosity increased under fully ice-saturated conditions. Since P-wave, SH-wave, and SV-wave velocities were utilized to calculate the elastic modulus, the variations in

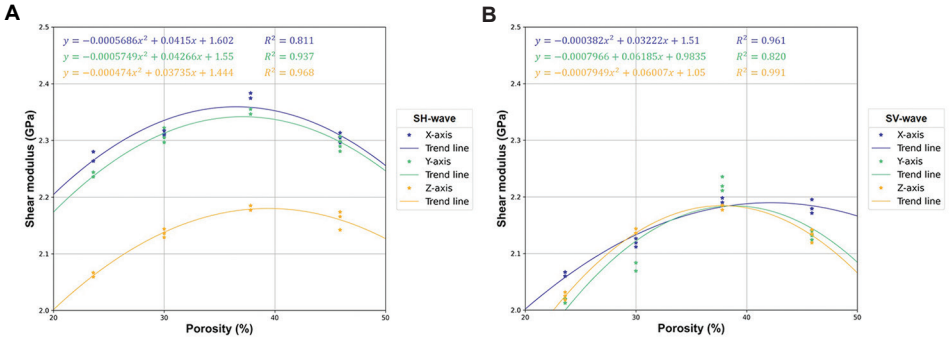

Figure 13. Shear modulus versus porosity in the permafrost simulation model calculated using (A) shear-horizontal (SH)-wave and (B) shear-vertical (SV)-wave velocities. The trend lines were generated using a second-order polynomial. Blue, green, and yellow markers represent the shear modulus measured along the X-, Y-, and Z-axes, respectively.

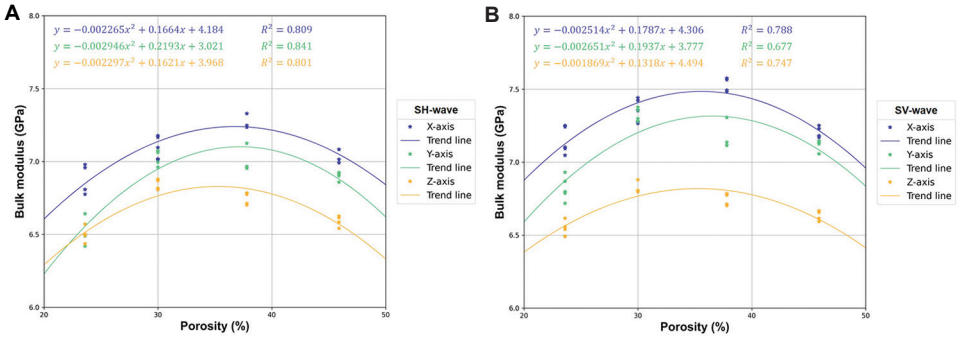

Figure 14. Bulk modulus versus porosity in the permafrost simulation model calculated using (A) shear-horizontal (SH)-wave and (B) shear-vertical (SV)-wave velocities. The trend lines were generated using a second-order polynomial. Blue, green, and yellow markers represent the shear modulus measured along the X-, Y-, and Z-axes, respectively.

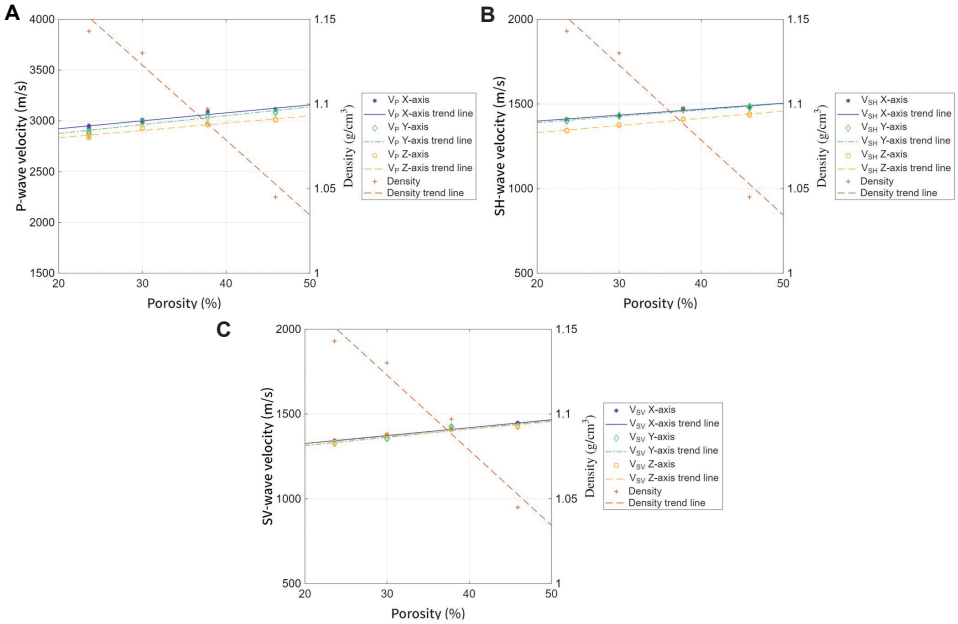

Figure 15. Relationships between seismic velocity/density and porosity in the permafrost simulation model. (A) P-wave velocity. (B) Shear-horizontal (SH)-wave velocity. (C) Shear-vertical (SV)-wave velocity. Blue, green, and yellow markers/lines represent the seismic wave velocities/trend lines along the X-, Y-, and Z-axes, respectively. The orange markers/lines represent the density/density trend lines.

velocity and density with respect to porosity were analyzed separately for each wave type. With increasing porosity, the seismic velocity increased due to the reinforcing effect of ice filling the larger pore volumes. In contrast, the overall density of the model decreased as porosity increased, attributable to the added pore volume reducing the bulk density of the material despite the presence of ice. Notably, the point of intersection between the seismic velocity and density trends corresponds to the porosity at which the elastic modulus begins to decline. This suggests that at low porosities, the increase in seismic velocity dominates the modulus calculation, increasing the elastic modulus. However, beyond a critical porosity, the reduction in density becomes the dominant factor, leading to a decrease in the elastic modulus despite the continued increase in velocity.

The effect of freezing was analyzed to understand its influence on the elastic behavior of the permafrost simulation model. When water within the pore spaces freezes, it undergoes a phase change accompanied by volume expansion. This freezing-induced expansion plays a complex role in determining the elastic modulus, as it can contribute to either strengthening or weakening of the material, depending on the porosity and structural response of the model.

In cases where the pore volume is limited, such as in low-porosity models, the expansion of ice during freezing

can generate compressive stress on the surrounding solid matrix. This stress enhances particle interlocking and improves the overall structural integrity of the material, thereby increasing the elastic modulus. In essence, the expansion serves to bind the structure more tightly by exerting pressure on the grain contacts, leading to increased stiffness and rigidity.

However, when porosity is relatively high, the extent of ice expansion becomes more significant, which can exceed the mechanical tolerance of the surrounding particles. In such cases, the excessive internal pressure may induce microcracks within the solid particles or at the grain boundaries.[33,34] These microcracks act as zones of mechanical weakness, which degrade the material's stiffness and, consequently, reduce the elastic modulus.

Figure 16 presents a schematic diagram illustrating this mechanism, where excessive volume expansion caused by freezing leads to the development of microcracks in the particle structure. This explanation aligns with the trend seen in the experimental results: when porosity was low, the elastic modulus increased with increasing porosity; when porosity increased beyond the threshold, the elastic modulus decreased with increasing porosity.

5. Discussion

This study demonstrated the feasibility of using FDM-based 3D printing technology to fabricate permafrost simulation models with controlled porosity, enabling a systematic investigation of the relationship between porosity and elastic modulus. By overcoming the limitations of using natural rock cores, the proposed method provided an effective experimental method for studying the elastic modulus of permafrost with respect to porosity.

The key finding of this study is that the elastic modulus does not increase monotonically with porosity under fully ice-saturated conditions. Instead, the modulus increases up to a critical point, after which it begins to decline. This non-linear behavior is primarily attributed to two competing effects: (i) the increase in seismic velocity due to enhanced ice bonding within pore spaces at lower porosity levels, and (ii) the decrease in bulk density and potential formation of microcracks induced by freezing-related volumetric expansion at higher porosity levels. The intersection point of the velocity and density trends, as shown in Figure 15, aligns closely with the porosity at which the elastic modulus reaches its peak, supporting this interpretation.

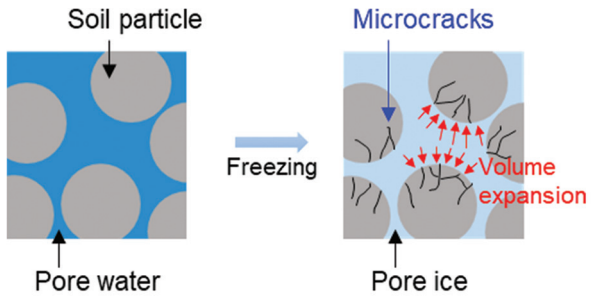

Figure 16. Schematic diagram of microcracks caused by ice volume expansion

These results highlight the dual role of freezing in permafrost systems. While ice formation can enhance the mechanical stiffness of the material by binding particles together, excessive ice expansion in high-porosity media may generate internal stresses that lead to microstructural damage, ultimately reducing the strength. This is quantitatively supported by the porosity measurements presented in Table 2. While the lower-porosity models (Models 1 and 2) exhibited negligible variations in porosity before and after freezing, the higher-porosity models (Models 3 and 4) showed more pronounced discrepancies. These deviations suggest that the internal stress generated by the volumetric expansion of ice caused structural damage in the high-porosity frameworks. Consequently, this induced damage is interpreted as the primary cause of the formation of microcracks and the subsequent decrease in elastic modulus observed beyond the critical porosity threshold.

The experimental method proposed here also opens the door for broader applications. By replacing ice with other fluids, such as water, oil, and brine, this technique can be used to study the porosity-dependent behavior of various saturated porous media. Moreover, varying the shape, size, and distribution of pores in models would allow for more comprehensive assessments of how pore architecture influences elastic properties.

Nevertheless, some limitations of the study should be acknowledged. The 3D-printed model, while effective for simulating elastic wave behavior, does not fully replicate the complex mineralogical and thermal properties of natural permafrost. In addition, freezing conditions in the experiment were static and uniform, whereas *in situ* freezing processes in natural environments are often dynamic and heterogeneous. Therefore, future research necessitates a comparative analysis between the results of laboratory experiments and those obtained from actual permafrost to bridge the gap between the simulation models and natural conditions. Furthermore, this study was conducted under conditions of complete ice saturation and zero salinity. However, natural permafrost often exhibits incomplete ice saturation and may contain saline pore water. Finally, although key properties such

as ice saturation, seismic velocity, and elastic moduli are sensitive to pressure and temperature changes, this study did not account for these environmental variables. Future research should incorporate more realistic boundary conditions, multi-phase modeling, and time-dependent effects to better simulate real-world permafrost behavior. In particular, further studies considering varying degrees of ice saturation, salinity, pressure, and temperature conditions are recommended to provide a more comprehensive analysis.

In summary, this study offers a novel experimental approach to permafrost research through the use of 3D printing and seismic physical modeling. It provides new insights into the mechanical response of frozen porous media and establishes a foundation for further research into the stability and geophysical characterization of permafrost environments.

6. Conclusion

This study proposed a method for controlling porosity and simulating permafrost using 3D printing. Furthermore, a permafrost simulation model with varying porosity was used in seismic physical modeling to analyze the elastic modulus according to porosity. The porosity of the permafrost simulation model was varied by controlling the number of pores and printed using an FDM 3D printer. The printed model was saturated with ice to simulate permafrost, and data were collected using seismic physical modeling. To analyze the elastic modulus according to porosity, seismic velocity was calculated from data obtained from seismic physical modeling. The results showed that the elastic modulus increased to approximately 38% of the porosity and then decreased, indicating the seismic wave velocity–density relationship and volumetric expansion due to freezing.

This study proposed a method utilizing 3D printing to overcome the limitations of controlling porosity in natural rock cores for permafrost research. Although the 3D-printed models differ from natural rocks, they demonstrate that the ice expansion within pores significantly affects the elastic modulus. From an engineering perspective, these findings provide a quantitative basis for evaluating the stability of infrastructure constructed on permafrost. By identifying the critical porosity threshold at which mechanical performance begins to degrade due to freezing expansion, engineers can better predict potential weakness zones and assess the bearing capacity of pipelines and foundations. Saturating the 3D-printed porous model, used as a permafrost simulation model, with fluids other than ice allows for the analysis of fluid properties associated with porosity. Varying pore structure and size enable systematic investigation into the effects of porosity within permafrost environments. Moreover, the applicability of this model further extends to studying permafrost degradation. By submerging the frozen model in water and controlling the temperature to induce gradual phase changes, the thawing process can be simulated. This approach allows for the monitoring of changes in elastic properties during the transition from frozen to thawed states, yielding valuable data for research on thawing environments. This approach may be extended to geological models, with potential applications in seismic exploration of permafrost regions.

Acknowledgments

None.

Funding

This research was supported by the Korea Institute of Marine Science and Technology Promotion (KIMST) funded by the Ministry of Oceans and Fisheries, Korea (RS-2023-00259633) and by the "Busan Regional Innovation System and Education (RISE)" Project supported by the Ministry of Education and Busan Metropolitan City (2025-RISE-02-002-012).

Conflict of interest

The authors declare that they have no competing interests.

Author contributions

Conceptualization: Daechul Kim, Sungryul Shin
Formal analysis: Yeonjin Choi
Investigation: Daechul Kim
Methodology: Wookeen Chung
Visualization: Daechul Kim
Writing–original draft: Daechul Kim
Writing–review & editing: Daechul Kim, Sungryul Shin

Availability of data

All data analyzed have been presented in the paper.

References

1. Van Everdingen RO, editor. *Multi-Language Glossary of Permafrost and Related Ground-Ice Terms in Chinese, English, French, German, Icelandic, Italian, Norwegian, Polish, Romanian, Russian, Spanish, and Swedish*. Germany: International Permafrost Association, Terminology Working Group; 1998.
2. Obu J. How much of the earth's surface is underlain by permafrost? *J Geophys Res Earth Surf*. 2021;126(5):2021JF006123.

   doi: 10.1029/2021JF006123

3. Schuur EA, McGuire AD, Schädel C, *et al*. Climate change and the permafrost carbon feedback. *Nature*. 2015;520: 171-179.

doi: 10.1038/nature14338

4. Biskaborn BK, Smith SL, Noetzli J, *et al*. Permafrost is warming at a global scale. *Nat Commun*. 2019;10:264.

doi: 10.1038/s41467-018-08240-4

5. Hjort J, Streletskiy D, Doré G, Wu Q, Bjella K, Luoto M. Impacts of permafrost degradation on infrastructure. *Nat Rev Earth Environ*. 2022;3:24-38.

doi: 10.1038/s43017-021-00247-8

6. Zhang Z, Zhang J, Chen J, Luo J, Lei B. Study on the stability of excavation process of permafrost subgrade slope in Alpine region. *Sci Rep*. 2025;15:4612.

doi: 10.1038/s41598-025-85651-6

7. Timur A. Velocity of compressional waves in porous media at permafrost temperatures. *Geophysics*. 1968;33(4): 584-595.

doi: 10.1190/1.1439954

8. Zimmerman RW, King MS. The effect of the extent of freezing on seismic velocities in unconsolidated permafrost. *Geophysics*. 1968;51(6):1285-1290.

doi: 10.1190/1.1442181

9. Dou S, Nakagawa S, Dreger D, Ajo-Franklin J. A rock-physics investigation of unconsolidated saline permafrost: P-wave properties from laboratory ultrasonic measurements. *Geophysics*. 2016;81(1):WA233-WA245.

doi: 10.1190/geo2015-0176.1

10. Li B, Matsushima J. Influence of ice properties on wave propagation characteristics in partially frozen soils and rocks: A temperature-dependent rock-physics model. *Geophysics*. 2024;89(5):MR281-MR295.

doi: 10.1190/geo2023-0694.1

11. Kurfurst PJ. Ultrasonic wave measurements on frozen soils at permafrost temperatures. *Can J Earth Sci*. 1976;13(11): 1571-1576.

doi: 10.1139/e76-163

12. Zhang R, Ding P, Zhang F, Li J. Innovative 2D ultrasonic reflection measurements in partially frozen unconsolidated sediment. *Geophysics*. 2025;90(4):MR295-MR306.

doi: 10.1190/geo2024-0657.1

13. ASTM International. *ISO/ASTM 52900:2015 Additive Manufacturing - General Principles - Terminology*. Washington, D.C: ASTM International; 2015.

doi: 10.1520/ISO ASTM 52900-15

14. Ishutov S, Hasiuk FJ, Harding C, Gray JN. 3D printing sandstone porosity models. *Interpretation*. 2015;3(3):SX49-SX61.

doi: 10.1190/INT-2014-0266.1

15. Ibrahim ER, Jouini MS, Bouchaala F, Gomes J. Simulation and validation of porosity and permeability of synthetic and real rock models using three-dimensional printing and digital rock physics. *ACS Omega*. 2021;6(47):31775-31781.

doi: 10.1021/acsomega.1c04429

16. Ding P, Zhang F, Li X, Chai Y. Analyzing the seismic response characteristics of P, SV, and SH waves to reservoir parameters using physical modeling. *Geophysics*. 2024;89(5):M109-M121.

doi: 10.1190/geo2023-0454.1

17. Ding P, Zhang F, Chai Y, Luo P, Gao L. Seismic physical modeling study for a shale oil reservoir with complex lithofacies and meter-scale structures. *Geophysics*. 2023;88(4):B179-B193.

doi: 10.1190/geo2022-0582.1

18. Huang L, Dyaur N, Stewart RR. Elastic properties of 3D-Printed physical models: fluid substitution observations in cracked media. In: *SEG Technical Program Expanded Abstracts 2015. Society of Exploration Geophysicists Annual Meeting Technical Program 2015*; 2015. p. 3100-3104.

doi: 10.1190/segam2015-5915204.1

19. Huang L, Stewart RR, Dyaur N, Franceschi JB. 3D-printed rock models: Elastic properties and the effects of penny-shaped inclusions with fluid substitution. *Geophysics*. 2016;81(6):D669-D677.

doi: 10.1190/geo2015-0655.1

20. Dande S, Stewart RR, Dyaur N. The effect of fluids and their viscosity on the elastic-wave velocity and anisotropy of 3D-printed VTI rock models. In: *SEG Technical Program Expanded Abstracts 2018. Society of Exploration Geophysicists Annual Meeting Technical Program 2018*; 2018. p. 347-350.

doi: 10.1190/segam2018-2998577.1

21. Dande S, Stewart RR, Dyaur N, Franceschi JB. The Effect of Proppant-Filled Fractures on the Elastic Properties of 3D-Printed Rock Models. In: *SEG Technical Program Expanded Abstracts 2017. Society of Exploration Geophysicists Annual Meeting Technical Program*; 2017. 2017. p. 5767-5771.

doi: 10.1190/segam2017-17789169.1

22. Wang J, Stewart RR, Dyaur NI. Seismic Response Analysis of a 3D-Printed Dual-Porosity Physical Model: Marine Case. In: *SEG Technical Program Expanded Abstracts 2018. Society of Exploration Geophysicists Annual Meeting Technical Program*; 2018. p. 301-305.

doi: 10.1190/segam2018- 2997200.1

23. Zerhouni O, Tarantino MG, Danas K. Influence of the Internal Geometry on the Elastic Properties of Materials

using 3D-Printing of Computer-Generated Random Microstructures. In: *SEG Technical Program Expanded Abstracts 2018*. *Society of Exploration Geophysicists Annual Meeting Technical Program 2018*; 2018. p. 3713-3718.

doi: 10.1190/segam2018-2998182.1

24. Kim D, Shin S, Chung W. *Analysis of Seismic Characteristics for Permafrost According to Porosity Ratio using 3D Printing Technology. Presented at*: *EGU General Assembly 2024*. Vienna, Austria: EGU24-7116; 2024.

doi: 10.5194/egusphere-egu24-7116

25. Pullan SE, MacAuley HA, Hunter JAM, Good RL, Gagne RM, Burns RA. Permafrost distribution determined from seismic refraction. In: Pelletier BR, editor. *Marine Science Atlas of the Beaufort Sea - Geology and Geophysics*. Miscellaneous Report 40. Ottawa: Geological Survey of Canada; 1987. p. 37.

doi: 10.4095/126940

26. Redwood B, Schoffer F, Garret B. *The 3D Printing Handbook Technologies, Design and Applications*. Netherlands: 3D HUBS; 2017.

27. Zhao Y, Wang L, Li H. Effect of freeze-thaw on the stability of a cutting slope in a high-latitude and low-altitude permafrost region. *Appl Syst Innov*. 2020;3(3):36.

doi: 10.3390/asi3030036

28. Syas'ko V, Shikhov A. Assessing the state of structural foundations in permafrost regions by means of acoustic testing. *Appl Sci*. 2022;12(5):2364.

doi: 10.3390/app12052364

29. Wyllie MRJ, Gregory AR, Gardner LW. Elastic wave velocities in heterogeneous and porous media. *Geophysics*. 1956;21(1):41-70.

doi: 10.1190/1.1438217

30. Birch F. The velocity of compressional waves in rocks to 10 kilobars: 2. *J Geophys Res*. 1961;66(7):2199-2224.

doi: 10.1029/JZ066i007p02199

31. Wang YH, Lo KF, Yan WM, Dong XB. Measurement biases in the bender element test. *J Geotech Geoenviron Eng*. 2007;133(5):564-574.

doi: 10.1061/(ASCE)1090-0241(2007)133:5(564)

32. Han Q, Wang Z, Teng Z, Zhang Y, Cao J. Analysis on "three-box" model of stress-strain in frozen soil porous media based on representative macroscopic Volume. *Front Earth Sci*. 2022;10:991384.

doi: 10.3389/feart.2022.991384

33. Carvalho FCS, Chen CN, Labuz JF. Measurements of effective elastic modulus and microcrack density. *Int J Rock Mech Min Sci*. 1997;34(3-4):43.e1-43.e11.

doi: 10.1016/S1365-1609(97)00239-6

34. Wang T, Jia H, Sun Q, Lu T, Tang L, Shen Y. Pressure melting of pore ice in frozen rock under compression. *Cold Reg Sci Technol*. 2023;210:103768.

doi: 10.1016/j.coldregions.2023.103856